Self-Commissioning Technique for High Bandwidth Servo Motor Drives

Yen-Shin Lai, *Fellow IEEE*
Center for Power Electronic Technology
National Taipei University of Technology
Taipei, Taiwan
yslai@ntut.edu.tw

Min-Hsien Ho
Center for Power Electronic Technology
National Taipei University of Technology
Taipei, Taiwan
t103318034@ntut.edu.tw

Abstract—The main theme of this paper is to propose a self-commissioning technique for high bandwidth servo drives. The presented self-commissioning technique include auto-identification of servo motor parameters and on-line calculation of controller gains of servo drives. The electrical parameters required for current controller, including stator resistance and inductance are identified under standstill. And followed by deriving the mechanical parameters for determining the speed and position controllers. The gains for *current controllers* are determined based upon the *magnitude optimal* method as the delay is considered while retaining the maximum phase margin. And the gains for speed controller are derived based upon symmetrical optimum method to increase the bandwidth as taking the current loop into consideration for speed gain design. Comparing with conventional self-commissioning method, the proposed method provides real alignment of rotor axis along the q-axis for q-axis inductance identification. Moreover, the proposed method gives significant bandwidth improvement of servo drives. Experimental results derived from DSP-controlled PMSM servo drives system will be shown. The results demonstrate high bandwidth servo drives can be achieved by the proposed self-commissioning technique. These results fully support the developed techniques and claims.

Keywords—component; Servo drives, Self-commissioning, Bandwidth

I. PRIOR ART AND OBJECTIVES

The advanced servo motor drives require well-tuned controller gains which are related to electrical and mechanical parameters of servo motors. In general, servo motor drives consist of current, speed and position control loops. To establish the gains of these loops, the motor electrical and mechanical parameters should be known in prior. Therefore, various self-commissioning and automatic control loop tuning methods have been proposed in recent years. High frequency signal injection method for inductance identification has been proposed in [1-2]. In [1], high frequency sinusoidal signal is injected as voltage reference in rotor reference frame and the induced current is extracted by the Discrete Fourier Transform (DFT) to calculate the inductance. In addition, the effect of inverter nonlinearities is considered, and an error model of inductance identification considering different rotor positions is used. Similarly, high frequency current injection method has been investigated in [2]. For a given amplitude and frequency of the injected high frequency current signal along with self-axis, the controller output voltage is observed. Since the frequency of the injected signal could be limited by the bandwidth of proportional-integral (PI) current controller, the standard PI controller is substituted by a PI controller plus resonant term (PI-RES) to enhance the current response. Furthermore, the voltage harmonics are eliminated by the real-time Fourier analysis. The saturation and cross-saturation effects are take into account during the inductance estimation. A self-commissioning scheme for electrical motor drives including elastic couplings and backlash is presented in [3]. In addition, particle swarm optimization (PSO) algorithm is used for identifying and optimizing the controller gains. While the controller optimization needs to tune the total inertia and friction coefficient of the system.

On-line parameter estimation methods are presented in [4-6]. In [4], an on-line inertia identification method based on fixed-order empirical frequency-domain optimal parameter (FOREFOP) has been proposed. To estimate the inertia more precisely, a load torque observer is employed. Disturbance torque observer with feedforward control for digital servo drives has been implemented in [5]. The inertia, viscous coefficient and constant disturbance torque are obtained by the relationship between torque components and the estimated disturbance torque. An on-line parameter identification method for both motor electrical and mechanical parameters based on recursive least squares (RLS) is presented in [6]. The electrical parameters are calculated by the voltage equation in discrete form and voltage drops on the inverter are considered. For the mechanical parameters estimation, torque equation is discretized and applied to the RLS algorithm. A self-commissioning scheme for induction motor drives with DTC control is proposed in [7]. However, back-EMF constant and torque constant were not discussed. Servo control loop tuning and parameter estimation method have been investigated in [8]. Winding resistor and inductances are estimated at standstill by injecting two pulsating voltages. However, the estimation accuracy of inductances and control loop bandwidth are not limited. For conventional inverter controller gain design [8] the bandwidth of current loop can be 1/10 of switching frequency. Similarly, the bandwidth of speed loop

978-1-5090-2998-3/17/$31.00 ©2017 IEEE

(position) is 1/10 of that for current (speed) loop. For the servo drives shown in Fig. 1, the conventional controller design approach gives the following results.

For q-axis current controller, the ratio of PI controller's time constant is set to motor electrical parameter, which is known as pole-zero cancellation. However, the bandwidth of the controller ω_i is assumed to be 1/10 of the switching frequency. Hence, proportional and integral gain of PI controller are given as

$$k_{p\_q} = \omega_i \cdot L_{qs} \tag{1}$$

$$K_{i\_q} = \omega_i \cdot R_s \tag{2}$$

The same rule is applied to speed loop controller design. Therefore, proportional and integral gain of speed PI controller is obtained by (3) and (4). Where ω_n is set to 1/10 of the bandwidth of current controller.

$$k_{q\_n} = \omega_n \cdot J_m \tag{3}$$

$$k_{i\_n} = \omega_n \cdot B \tag{4}$$

Generally, P controller is the most common used for position control. However, the closed-loop transfer function of position control loop is identical to a first-order low pass filter while the magnitude of the inner loop is assumed to be unity. Thus, position control gain is shown in (5).

$$k_{p\_p} = 0.1\omega_n \tag{5}$$

The merits of this conventional approach include *easy design controller* since the plant models for current, speed and position control gains design are simplified to a *first order transfer function*. However, this approach results in slow dynamic response. As shown in [8], for inverter with switching frequency = 5 kHz, the results of bandwidth are 500 Hz, 50 Hz and 5 Hz for the current, speed and position loops, respectively.

Based upon the survey of previous work, a self-commissioning technique for high bandwidth servo drives will be presented. Comparing with conventional self-commissioning method, the proposed method provides *real alignment* of rotor axis along the *q-axis* for q-axis inductance identification. Moreover, the gains for current controllers are determined based upon the magnitude optimal method as the delay is considered in the controller design while retaining the maximum phase margin. And the gains for speed controller are derived based upon symmetrical optimum method to increase the bandwidth as taking the current loop into consideration for speed gains design. Therefore, the proposed method gives significant bandwidth improvement of servo drives.

Experimental results derived from digital-controlled PMSM servo drives system will be shown. The proposed self-commissioning technique is confirmed using two motors for test. For the servo drives with switching frequency of 20 kHz, the achievable control bandwidth for the presented method of position control loop is improved from 20 Hz to 116 Hz. The results demonstrate the proposed self-commissioning of high bandwidth servo drives can be achieved by the proposed technique.

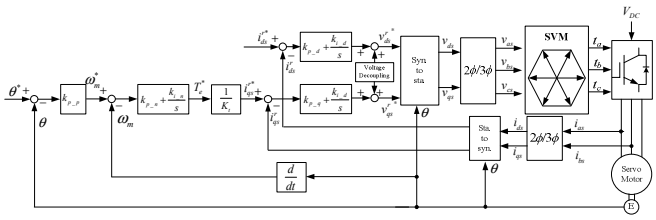

Fig. 1 Block diagram of servo drives

II. PROPOSED SELF-COMMISSIONING METHOD

A. Identification of Electrical Parameters

Fig. 2 shows the timing and signals (d-q axis voltage and current signals) for electrical parameters identification. As shown in Fig. 2, there are four periods for stator resistance calculation, d-axis inductance calculation, rotor alignment to q-axis and then q-axis inductance calculation. This electrical parameters identification process is realized in 600 ms as shown in Fig. 2. The special features of the proposed method as comparing with previous approach [8] include that the proposed method provides real alignment of rotor axis along the q-axis for q-axis inductance identification. This will improve q-axis inductance identification result. The electrical parameters of servo motors are calculated by:

$$\hat{R}_s = \frac{v^2_{ds\_Rs} - v^2_{ds\_Rs}}{i^2_{d\_Rs} - i^1_{d\_Rs}} \tag{6}$$

$$\hat{L}_{ds} = \frac{\left[\left(v^{r2}_{ds} - v^{r1}_{ds}\right) - \hat{R}_s\left(\Delta i^{r2}_{ds} - \Delta i^{r1}_{ds}\right)\right]\times\Delta t}{\left(\Delta i^{r2}_{ds} - \Delta i^{r1}_{ds}\right)} \tag{7}$$

$$\hat{L}_{qs} = \frac{\left[\left(v^{r2}_{qs} - v^{r1}_{qs}\right) - \hat{R}_s\left(\Delta i^{r2}_{qs} - \Delta i^{r1}_{qs}\right)\right]\times\Delta t}{\left(\Delta i^{r2}_{qs} - \Delta i^{r1}_{qs}\right)} \tag{8}$$

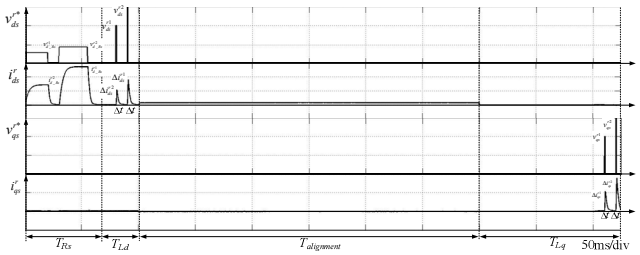

Fig. 2 Timing and signal for electrical parameters identification

B. Calculation of Current Control Gains

Fig. 3 illustrates the current control loop using q-axis current as an example. However, the motor electrical model, including stator resistor and inductance give the motor electrical time constant. K_{PI} and T_{NI} are PI controller's gain and time constant, respectively. The system delay $T_{\Sigma I}$, includes

current sampling delay, T_{fb}, and the calculation delay, T_{proc} and PWM switching active delay, T_{PWM}. Thus, the overall delay $T_{\Sigma I}$ is shown in (9). Time constant of current controller are set to motor electrical time constant, which is known as open-loop shaping and thus, open loop transfer function is shown in (10). However, to simplify the transfer function further, two normalized coefficients are introduced. One is control gain related, γ, and the other is frequency related, Ω, as shown in (11). Hence, open loop transfer function can be rewritten by substitute the normalized coefficients into (10) and given in (12). Considering the delay in the plant model and derive the controller gains based upon the magnitude optimum method [9] for the given phase margin = 61 degrees and γ =0.5, the controller gain K_{PI} and time constant T_{NI} can be derived as shown in (13) and (14). While the bandwidth is defined as the frequency at which the phase angle passed through 90°[13], and the relationship between γ and $\Omega_{B\phi}$ is derived in (15). Similarly, the d-axis current controller gains can be derived as the d-axis inductance is given.

$$T_{\Sigma I} = T_{fb} + T_{proc} + T_{PWM} \tag{9}$$

$$F_{OI}(s) = \frac{K_{PI}}{L_{qs}} \frac{e^{-T_{\Sigma I}}}{s} \tag{10}$$

$$\begin{cases} \gamma = \dfrac{K_{PI} T_{\Sigma I}}{L_s} \\ \Omega = \omega T_{\Sigma I} \end{cases} \tag{11}$$

$$F_{OI}(j\Omega) = \gamma \frac{e^{-j\Omega}}{j\Omega} \tag{12}$$

$$K_{PI} = 0.5 \frac{L_{qs}}{T_{\Sigma I}} \tag{13}$$

$$T_{NI} = \frac{L_{qs}}{R_s} \tag{14}$$

$$\gamma = \Omega_{B\phi} \sin \Omega_{B\phi} \tag{15}$$

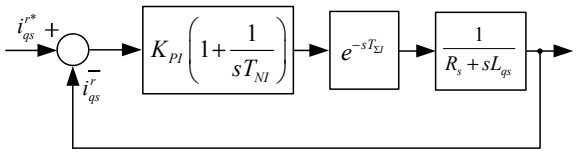

Fig. 3 q-axis current controller

C. Identification of Mechnical Parameters

As the current controller gains are derived, current control is applied during the identification process of mechanical parameters as shown in Fig. 4. A q-axis current reference is given at $t=t_0$, the motor will accelerate to steady state at $t=t_2$. Then, the q-axis current starts to decrease since the dc-link voltage is no longer larger than the back EMF. Therefore, the torque constant $\hat{k}_t$ can be derived as shown in (16) [10]. Frictional coefficient $\hat{B}$ is obtained based upon motor torque equation and given in (17). Run-out test [11] is applied to identify the system inertia. As illustrated in Fig. 4, motor is rotating in a constant speed at the interval [t_1, t_2]. However, PWM drive signal is switched off at $t=t_2$, and the motor is decelerated by the loss of driving torque with speed measured as a function of time. Thereby, inertia $\hat{J}$ can be calculated by solving the torque equation as a linear differential equation and shown in (18)[11].

$$\hat{k}_t = \frac{3}{2}\left[\frac{v_{qs}^{r*} - i_{qs}^{r}(\hat{R}_s + s\hat{L}_q)}{\omega_m}\right] \tag{16}$$

$$\hat{B} = \frac{i_{qs}^{r} \times \hat{k}_t}{\omega_m} \tag{17}$$

$$\hat{J} = \frac{-\hat{B}(t-t_2)}{\ln \dfrac{\omega_m(t)}{\omega_m(t_2)}},\ t_2 < t < t_3 \tag{18}$$

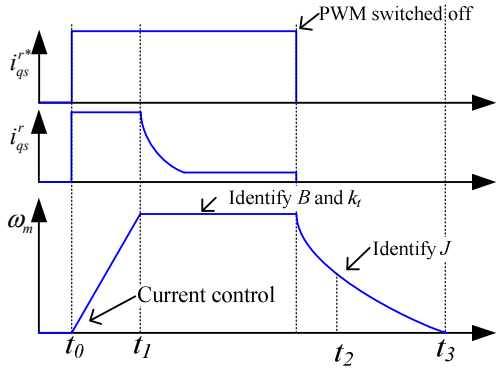

Fig. 4 Timing and signal for mechanical parameters identification

D. Calculation of Speed and Position Controller Gains

Speed control loop can be modeled as shown in Fig. 5. K_{PN} and T_{NN} depict the gain of speed PI controller and time constant, respectively. Motor mechanical model can be modeled as a system inertia J resulting in an integrator. T_{TN} is the required calculation time of speed control algorithm. Time constant of speed filter is designated as T_{FN}. The inner loop, current control loop, is represented by the closed loop transfer function F_{WI}. Therefore, the open loop transfer function $F_{ON}(s)$ can be written as (19).

$$F_{ON}(s) = K_{PN}\left(1 + \frac{1}{sT_{NN}}\right) \frac{F_{WI}(s)}{sJ} \frac{e^{-sT_{TN}}}{1+sT_{FN}} \tag{19}$$

However, the controller's parameters K_{PN} and T_{NN} can be derived based on symmetrical optimum [11-12], which is a standard design criterion for transfer function including double integrators. The total speed loop delays can be summed up into one term as shown in (20). Based on this simplification, the open loop transfer function $F_{ON}(s)$ can be rewritten as (21).

$$T_{\Sigma N} = T_{EI} + T_{FN} + T_{TN} \tag{20}$$

$$F_{ON}(s)=\frac{K_{PN}(1+sT_{NN})}{s^2JT_{NN}(1+sT_{\Sigma,N})} \tag{21}$$

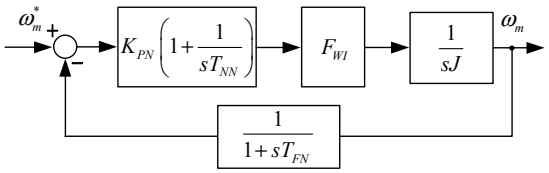

Fig. 5 Speed control loop

The crossover frequency of $F_{ON}(s)$ is given in (22). Once the crossover frequency is derived, a constant "α" is introduced since the main idea of symmetrical optimum is to choose the crossover frequency at the geometric mean of the two corner frequencies[11-12] and thus, the maximum phase margin can be achieved, as shown in Fig. 6. Three different cases of α is presented in Fig. 7. Apparently, α is proportional to phase margin and typically lies in a scale of 2 to 4. However, based on symmetrical optimum design rule, the controller gain and time constant of speed controller are given in (23) and (24)[9,11-12], respectively. Speed closed loop transfer function $F_{WN}(s)$ is given in (25).

$$\omega_{cN}=\frac{1}{\sqrt{T_{NN}T_{\Sigma N}}} \tag{22}$$

$$K_{PN}=\frac{J}{\alpha T_{\Sigma,N}} \tag{23}$$

$$T_{NN}=\alpha^2 T_{\Sigma,N} \tag{24}$$

$$F_{WN}(s)=\frac{(1+sT_{NN})}{\frac{JT_{NN}T_{\Sigma N}}{K_{PN}}+\frac{JT_{NN}}{K_{PN}}s^2+T_{NN}s+1} \tag{25}$$

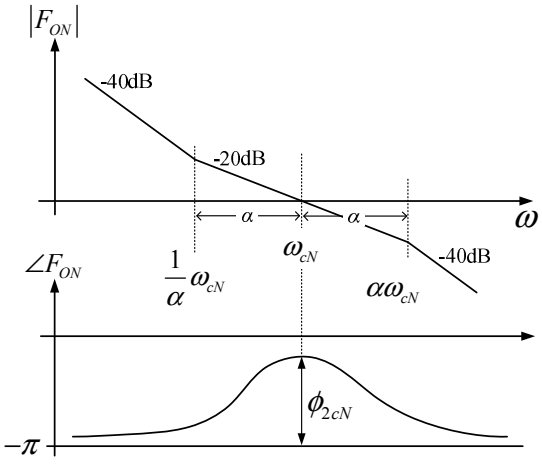

Fig. 6 Bode diagram according to symmetrical optimum

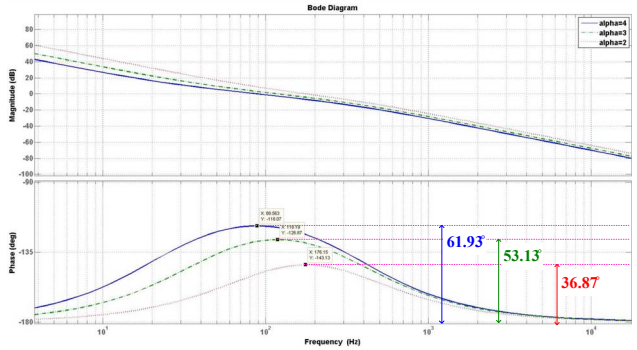

Fig. 7 Bode plot of $F_{ON}(s)$ with different α

The position control loop is consisting of speed closed loop $F_{WN}(s)$, position gain K_{PP} and an integrator, as shown in Fig. 8. Before derive position control gain K_{PP}, it should be noted that significant overshoot dose exists due to the double integration term in the open loop transfer function $F_{ON}(s)$.

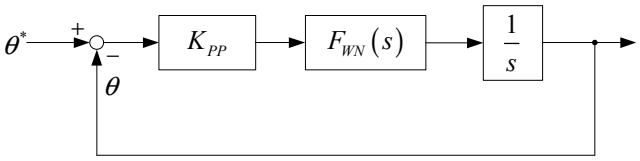

Fig. 8 Position control loop

Although the transient performs well damping, the step response is still characterized by a considerable overshoot. To eliminate the overshoot, a low pass filter can be cascaded with the speed reference and as illustrated in Fig. 9. If the time constant of low pass filter T_σ is set to T_{NN}, the modified speed closed loop transfer function gives as follow:

$$F_{WN}'(s)=\frac{\omega_m}{\omega_m^{*\prime}}=\frac{1}{\frac{JT_{NN}T_{\Sigma N}}{K_{PN}}s^3+\frac{JT_{NN}}{K_{PN}}s^2+T_{NN}s+1} \tag{26}$$

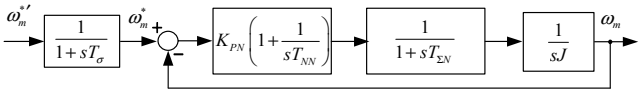

Fig. 9 Speed loop with LPF

Obviously, the overshoot is eliminated while the closed speed loop is cascaded with a low pass filter, and the Bode plot of $F_{WN}(s)$ and $F_{WN}'(s)$ are indicated by the solid and dash line in Fig. 10, respectively.

Based on this strategy and assume the magnitude of $F_{WN}(s)$ is unity, the simplified position control loop is shown in Fig. 11. The position closed loop transfer function $F_{WP}(s)$ is derived as (27). Hence, the position control gain K_{PP} can be determined in accordance with the cutoff frequency of the low pass filter which is used to eliminate the speed overshoot and given in (28).

$$F_{WP}(s) = \frac{K_{PP}}{s + K_{PP}} \tag{27}$$

$$K_{PP} = \frac{1}{T_{NN}} \tag{28}$$

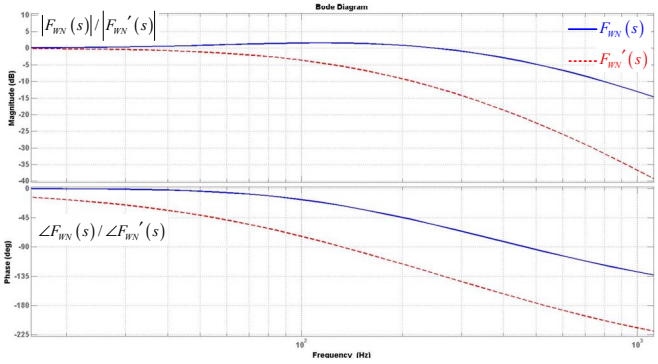

Fig. 10 Bode plot of $F_{WN}(s)$ and $F_{WN}'(s)$

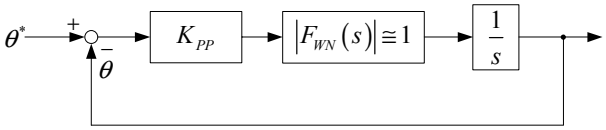

Fig. 11 Modified position control loop

III. EXPERIMENTAL RESULTS

Experimental results will be presented in this section to verify the parameter identification methodology and theoretical analysis of servo controllers. Block diagram of servo motor drive is shown in Fig. 12. Servo controllers, including current, speed and position controllers are digitalized via Renesas RZ/T1 R7S910017. Fig. 13 demonstrated the test platform for experimental verification. DC link voltage and switching frequency are set to 155V and 20 kHz.

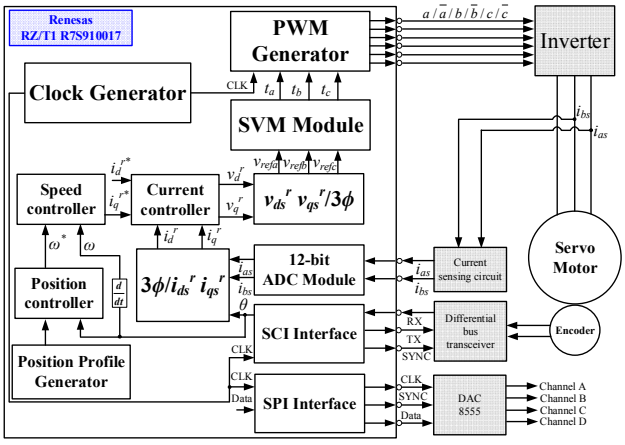

Fig. 12 Block diagram of servo motor drive

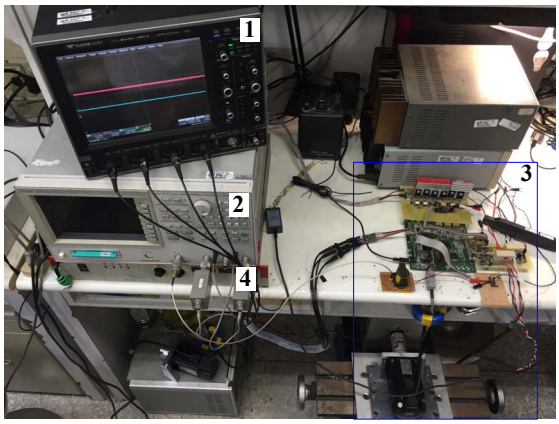

Fig. 13 Test platform for experimental verification

A. *Experimental Results for parameters identificatoin*

Self-commissioning methodology that investigated in this paper has been applied to two servo motors. The specifications of servo motor I are listed on Table 1 and II, respectively.

Table I. SPECIFICATIONS OF MOTOR I

TSC08751C-3NN33-D		
Items	Value	Unit
P_r	750	W
i_r	4	A
N	3000	rpm
Pole	8	-

Table II. SPECIFICATIONS OF MOTOR II

SMH-L040R30TSA		
Items	Value	Unit
P_r	400	W
i_r	2.4	A
N	3000	rpm
Pole	8	-

The estimation process of $\hat{R}_s$, $\hat{L}_d$ and $\hat{L}_q$ for Motor I are depicted in Fig. 8. However, the whole parameters identification procedure is illustrated in Fig. 14. Note that, once all the parameters are identified, a servo control with S-curve profile is given and as shown in Fig. 14. The comparison between estimated parameters and manual measured one for Motor I are listed in Table III.

TABLE III. PARAMETERS COMPARISON OF MOTOR I

	Manual	Self-commissioning	Error(%)
R_s (Ω)	1.06	1.145	7.5
L_d (*H*)	3.19	3.05	4.4
L_q (*H*)	3.875	3.87	0.13
J (kgm^2)	0.76 m	0.694 m	8.6
B(Nm/rad/s)	0.531 m	0.57 m	7.3
k_e(V/rad/s)	0.292	0.29	0.6
k_t(Nm/A)	0.438	0.43	1.8

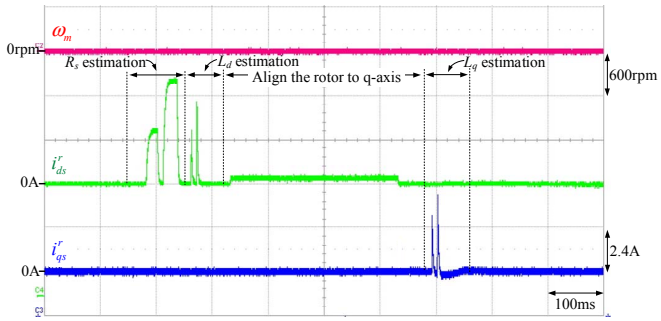

Fig. 14 Estimation process of R_s, L_d and L_q for Motor I

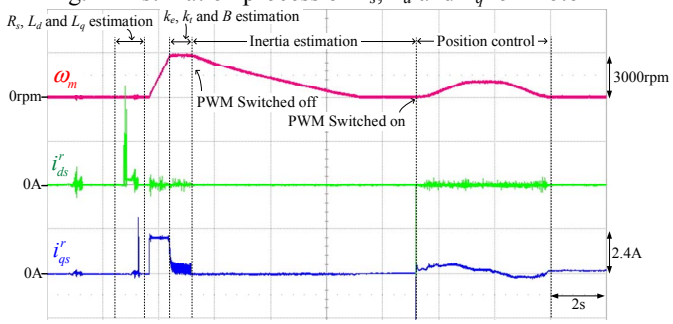

Fig. 15 Self-commissioning process for Motor I

Identification process of $\hat{R}_s$, $\hat{L}_d$ and $\hat{L}_q$ for Motor II are shown in Fig. 16, and the entire parameters estimation process and position control are given in Fig. 17. Nevertheless, the estimated parameters and manual measured one for Motor II are compared in Table IV.

TABLE IV. PARAMETERS COMPARISON OF MOTOR II

	Manual	Self-commissioning	Error(%)
R_s (Ω)	2.05	2.18	6.3
L_d (mH)	6.4	6.186	3.3
L_q (mH)	7.89	8.65	9.6
J (kg-m^2)	0.58 m	0.613m	5.8
B (Nm/rads^{-1})	0.34 m	0.327 m	6.5
k_e (V/rads^{-1})	0.282	0.2924	1.8
k_t (Nm/A)	0.423	0.4386	2.5

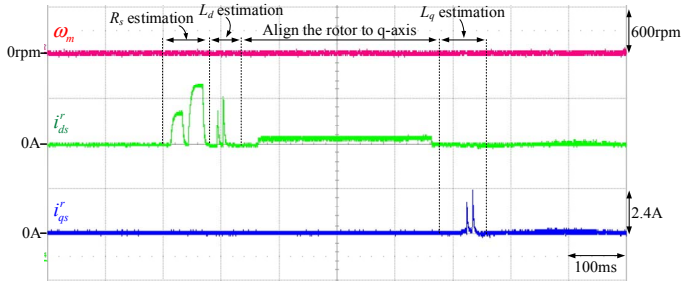

Fig. 16 Estimation process of R_s, L_d and L_q for Motor II

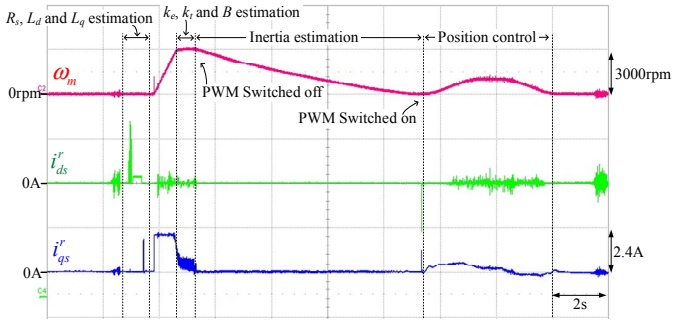

Fig. 17 Self-commissioning process for Motor II

B. Experimental Result of Servo Control Algorithm

The current regulation performance is shown in Fig. 18 and notes that the rotor should be locked. The q-axis current reference is regulated with a sinusoidal wave. The magnitude, offset and frequency of the current reference are set to 0.5A, 1A and 2850Hz. It can be seen that the phase lag between current response and reference is 89.6 degrees. Speed regulation performance is performed in Fig. 19 with sinusoidal excitation. The amplitude and frequency of the speed reference are given as 100 rpm and 400 Hz, respectively. Apparently, the amplitude of speed response is decayed by 3dB. Fig. 20 depicts the position regulation performance. However, the magnitude of position reference is 0.1 rad and the frequency is 100Hz. Position response is attenuated by 3dB as shown in Fig. 20. Bode plots of current, speed and position control loop are given in Fig. 21 to 23. While the solid line indicates the tested one by network analyzer, and the dash line points out the simulated one. Servo control with S-curve profile is shown in Fig. 24, and the displacement and maximum velocity are set tot 100 rad and 83 rad/s respectively.

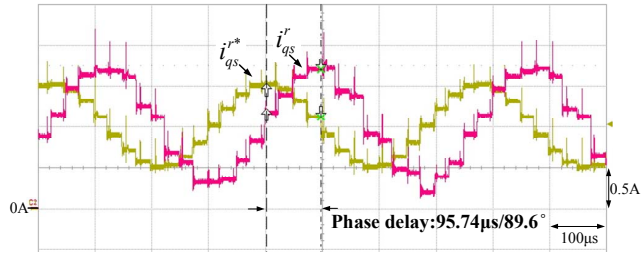

Fig. 18 Current loop bandwidth verification by sinusoidal excitation

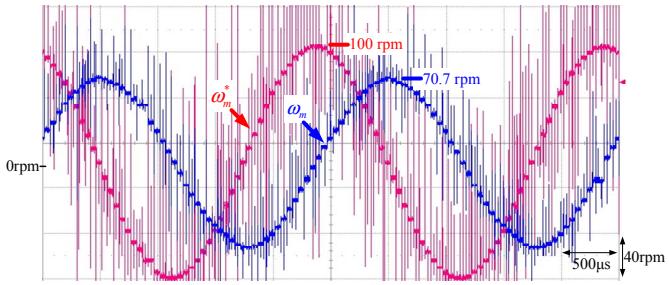

Fig. 19 Speed loop bandwidth verification by sinusoidal excitation

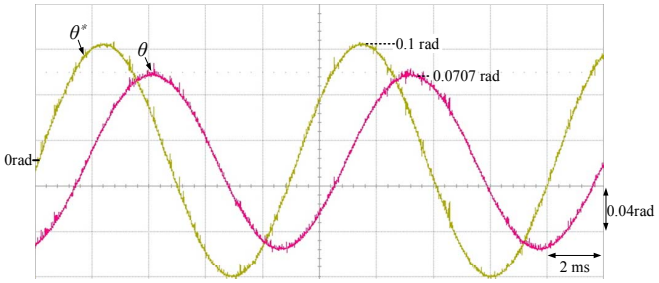

Fig. 20 Position loop bandwidth verification by sinusoidal excitation

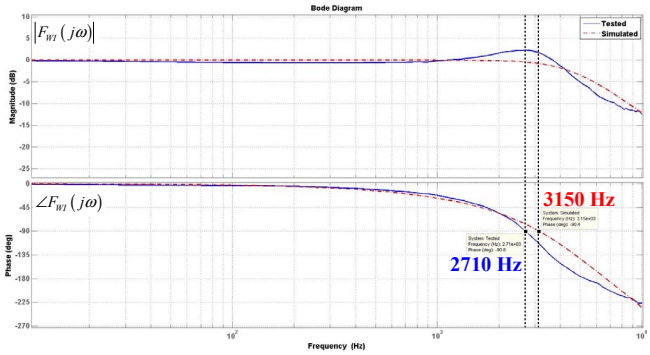

Fig. 21 Simulated and tested bandwidth of current control loop

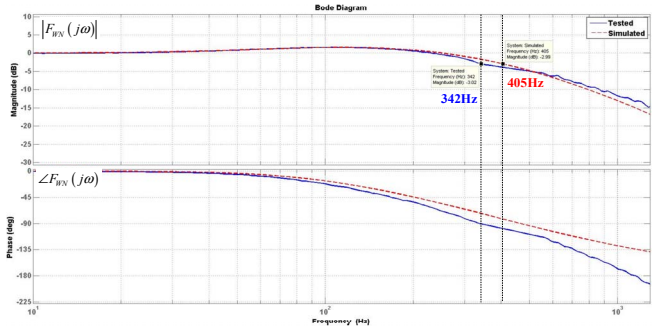

Fig. 22 Simulated and tested bandwidth of speed control loop

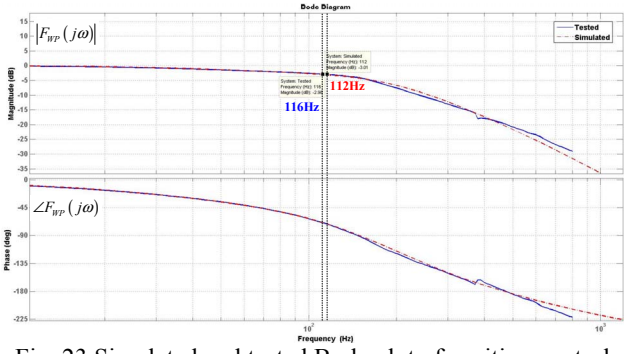

Fig. 23 Simulated and tested Bode plot of position control loop

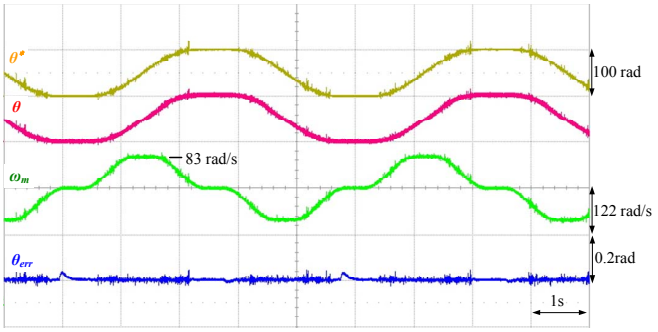

Fig. 24 Servo control with S-curve profile

IV. CONCLUSIONS

A simple self-commissioning scheme and controller tuning methods for servo motor drives are presented in this paper. Note that the investigated parameter estimation method without needing complicated methodology and the estimation error is less than 10%. However, servo controller design method are presented as well. Theoretical derivation, simulation results and experimental results are provided. Experimental results for servo controller bandwidth verification are summarized in Table V. Servo controller bandwidth is verified by two methods, one is sinusoidal excitation and the other is network analyzer. The bandwidth of position control loop is improved from 20Hz to 116Hz. Experimental results fully support the claims.

TABLE V. Summary of servo controller bandwidth verification

	Simulated Bandwidth	Tested Bandwidth	Network Analyzer
Current loop	3140Hz	2850Hz	2710Hz
Speed loop	405Hz	400Hz	342Hz
Position loop	112Hz	100Hz	116Hz

ACKNOWLEDGMENT

REFERENCES

[1] G. Wang, L. Qu, H. Zhan, J. Xu, L. Ding, G. Zhang, and D. Xu "Self-commissioning of permanent magnet synchronous machine drives at standstill considering inverter nonlinearities," IEEE Transactions on Power Electronics, vol. 29, no. 12, pp. 6615-6627, Dec. 2014.

[2] S. A. Odhano, P. Giangrande, R. Bojoi, and C. Gerada, "Self-commissioning of interior permanent-magnet synchronous motor drives with high-frequency current injection," IEEE Transactions on Industry Electronics, vol. 40, no. 5, pp. 3295-3303, Sep. 2014.

[3] M. Calvini, M. Carpita, A. Formentini and M. Marchesoni, "PSO-based self-commissioning of electrical motor drives," IEEE Transactions on Industrial Electronics, vol. 62, no. 2, pp. 768-776, Feb. 2015.

[4] L. Niu, D. Xu, M. Yang, X. Gui, and Z. Liu, "On-line inertia identification algorithm for PI parameters optimization in speed loop," IEEE Transactions on Power Electronics, vol. 30, no. 2, pp. 849-859, Feb. 2015.

[5] S. Kobayashi, I. Awaya, H. Kuromaru and K. Oshitani, "Dynamic model based auto-tuning digital servo driver," IEEE Transactions on Industrial Electronics, vol. 42, no. 5, pp. 462-466, Oct. 1995.

[6] D. Tadokoro, S. Morimoto, Y. Inoue and M. Sanada, "Method for auto-tuning of current and speed controller in IPMSM drive system based on

parameter identification," in Proc. of the International Power Electronics Conference, Hiroshima, pp. 390-394, 2014.

[7] Y. S. Lai, J. C. Lin and J. S. Wang, "Direct torque control induction motor drives with self-commissioning based on taguchi methodology," IEEE Transactions on Power Electronics, vol. 15, no. 6, pp. 1065-1071, Nov. 2000.

[8] S. M. Yang, and K. W. Lin, "Automatic control loop tuning for permanent magnet ac servo motor drives," IEEE Transactions on Industrial Electronics, vol. 63, no. 3, pp. 1499-1506, Mar. 2016.

[9] J. Böcker, S. Beineke and A. Bähr, "On the control bandwidth of servo drives," EPE 2009, Barcelona, Spain.

[10] K. W. Lee and J. I. Ha, "Evaluation of back-EMF estimators for sensorless control of permanent magnet synchronous motors," Journal of Power Electronics, vol. 12, no. 4, pp. 604-614, Jul. 2012.

[11] W. Leonhard, Control of Electrical Drives, 3rd edition, Springer, 2001.

[12] D. Schröder, "SchrElektrische Antriebe - Regelung von Antriebssystemen," 3rd edition, Springer 2009.

[13] J. H. Lumkes, Control Strategies for Dynamic Systems, New York: Marcel Dekker, 2002.